RSC Advances

ROYAL SOCIETY OF CHEMISTRY

www.rsc.org/advances

Magnetic core-shell nanoprobe for sensitive killing of cancer cells via induction with strong external magnetic field

Running Title: Magnetic core-shell nanoparticle induce cancer cell death

Samir Mandal[†], Nabanita Chatterjee[‡], Subhadip Das[‡], Krishna Das Saha[‡], and Keya Chaudhuri[†]*

[†]Molecular and Human Genetics Division and [‡]Cancer Biology and Inflammatory Disorder Division, CSIR-Indian Institute of Chemical Biology, Kolkata 700032, India

*Corresponding author

Dr. Keya Chaudhuri

Molecular and Human Genetics Division

CSIR-Indian Institute of Chemical Biology

4, Raja S.C. Mullick Road, Kolkata-700 032, India.

Tel: 91-33-2473-0350; Fax: 91-33-2473-5197

Email: keya.chaudhuri@gmail.com

kchaudhuri@iicb.res.in

Abstract

The title system, composed of a highly magnetic core surrounded by a thin arsenite shell, has been synthesized and applied to the magnetically facilitated targeting of anticancer agent (sodium arsenite) into human hepatocellular liver carcinoma cells (HepG2) for exploiting arsenite at lower dose with minimal side effect and higher efficacy by biocompatible manner. More specifically, we could achieve significantly higher apoptosis efficiency by targeting our sodium arsenite containing magnetic core-shell nanoparticles (MCNP) to HepG2 cells by external magnetic field and a putative pathway was established on the basis of ROS (reactive oxygen species) generation assay, cell cycle analysis, mitochondrial membrane potential determination and nuclear localization of p53. This study first indicates the association of p53 with arsenic containing MCNP-induced hepatocellular apoptosis in presence of external magnetic field through modulation of specific signaling-pathways. This MCNP-based drug targeting method therefore can potentially be a powerful tool for the advanced treatment of various cancers.

1. Introduction

Arsenicals for thousands of years have been known to act as carcinogens or poison. Paradoxically, however, arsenicals have also been known to have a wide range of therapeutic applications or beneficial effects including anti-cancer activity. Currently, arsenic trioxide (ATO) is considered an effective frontline treatment for relapsed and/or refractory APL patients and has been approved by the Food and Drug Administration (FDA) for general treatment of APL. In this regard, numerous reports highlight the potency of arsenic in a variety of hematological malignancies such as chronic myelogenous leukemia, promonocytic leukemia, T-cell leukemia, multiple myeloma and a large variety of cancers of solid tumor origin like neuroblastoma, glioblastoma, renal cell carcinoma, transitional cell cancer, gastric,

head and neck, cervical, hepatocellular, prostate and breast cancer [1-8]. ATO has been used as single agent or in combination with other drugs of choice for each particular disease.

Our previous studies have shown that the soluble most toxic and naturally prevalent form of arsenic ($NaAsO_2$) resulted in the induction of apoptosis in vitro in human malignant melanoma cell line A375 at higher dose with respect to the maximum tolerance dose limit of $NaAsO_2$ [9]. Increases in reactive oxygen species (ROS) production, loss of mitochondrial membrane potential associated with an activation of caspases was found to be the critical mediators of apoptosis. However, diverse sensitivity of tumor cells to higher dose of arsenic limits its extensive clinical application [10, 11]. In addition, sensitization of less sensitive cells requiring up to 10-fold higher dose of arsenic is not clinically achievable without the risk of arsenic-mediated side effects or damage to normal cells limiting its clinical efficacy [11]. As a result, most advanced cancers, especially solid tumors, are not curable yet by arsenic therapy alone. Consequently, it is desirable to exploit arsenite at lower dose with minimal side effect and higher efficacy. This could be done excellently by the help of nanotechnology.

Herein, we describe the synthesis of well-defined magnetic core-shell nanoparticles (MCNPs), composed of a magnetic core (Fe_3O_4) surrounded by a thin arsenite shell ($NaAsO_2$), and their delivery into human hepatocellular liver carcinoma (HepG2) cells in a highly efficient and external magnetically controlled manner (Fig. 1). Specifically, we could achieve significantly higher apoptosis efficiency by targeting our MCNP to HepG2 cells by external magnetic field and a putative pathway was established on the basis of ROS (reactive oxygen species) generation assay, cell cycle analysis, mitochondrial membrane potential determination and nuclear localization of p53.

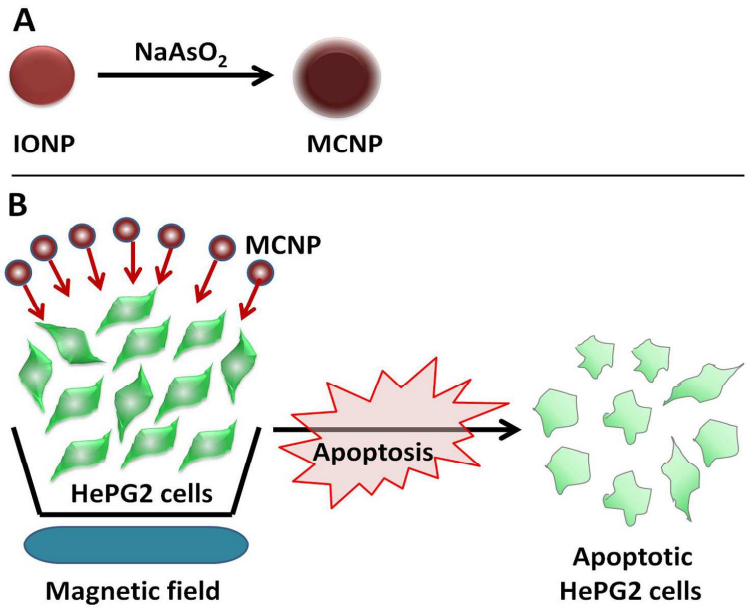

Fig. 1 Schematic representation of the synthesis of MNCP and their application for targeting the cancer cells. A) Generation of MCNPs. B) Magnetically facilitated arsenite delivery using MCNPs to kill the cancerous cells through apoptosis.

2. Experimental procedures

2.1. Synthesis and purification of iron oxide nanoparticles

Iron oxide nanoparticles (IONPs) were synthesized by a modified co-precipitation method. Ferrous chloride ($FeCl_2.4H_2O$, 0.5 g) was dissolved in 20 ml of 1M HCl with stirring, followed by addition of ferric chloride ($FeCl_3.6H_2O$, 1.35 g). Entire reaction mixture was then well mixed by stirring and heating at 450C under Argon atmosphere to prevent unwanted oxidation. Subsequently, 20 ml of 3M NaOH was added, resulting in a black precipitate and the reaction was continued at 450C for 30 min. The black precipitate was separated by using magnetic field and washed four times with 30 ml deionized and deoxygenated water. Finally the black precipitate was dispersed in 20 ml of citric acid-sodium citrate buffer. The excess citrate was removed from the IONP solution by repeated

centrifugation and washing with deionized and deoxygenated water. Finally the IONPs were redispersed in HPLC grade water for storing.

2.2. Synthesis of arsenite loaded magnetic core-shell nanoparticles (MCNP)

Arsenite coating on to the surface of magnetic iron oxide nanoparticles was done by slow addition of 50 mM sodium arsenite ($NaAsO_2$) solution into a sealed conical flux containing 10 ml of IONP solution (0.5 g of IONP) under stirring condition with nitrogen atmosphere. After the complete addition of sodium arsenite solution, the reaction mixture was allowed to stirring and heating at 72^0C for 2 h. The unbound arsenite was removed by repeated centrifugation at 32,000 rpm for 30 min and washing with HPLC grade water.

2.3. Dynamic light scattering

Dynamic light scattering (DLS; MAL1030323; Malvern Instrument Ltd., UK) was employed to determine the average size of the IONPs. A dilute solution of the nanoparticles was prepared by adding double distilled water and the experiment was carried out applying cuvette with uniform wall.

2.4. Atomic force microscopy

Sample for Atomic Force Microscopy (AFM) was prepared by dropping 10 µl of nanoparticle solution onto a freshly cleaved muscovite Ruby mica sheet (ASTM V1 Grade Ruby Mica from MICAFAB, Chennai). The molecules not firmly attached to the mica surface were removed by gently washing with nano-free double distilled water. Finally the nano-coated mica sheet was dried under vacuum and subjected to imaging [12, 13]. The synthesized nanoparticles were visualized by AAC mode using a Pico plus 5500 AFM (Agilent Technologies USA) with a piezoscanner at maximum range of 9 µm.

2.5. X-ray diffraction analysis

The phase identification of the synthesized IONPs was carried out by X-ray diffraction analysis (Philips PW1710) using Cu Kα radiation (λ=1.5406 A). A thin film of the powder was deposited on a glass plate for X-ray analysis.

2.6. FTIR spectroscopy

The FT-IR spectra of the samples were recorded on a JASCO FT/IR 4200 spectrometer using the (KBr) disc technique. The IONPs were mixed with KBr in a clean glass pestle and mortar and compressed to obtain a pellet. The spectra were recorded from 400–4000 cm^{-1}. Background spectra were obtained with a KBr pellet for each sample. JASCO software was used for data processing.

2.7. Cell culture and treatment

Human hepatocellular liver carcinoma cell line (HepG2), utilized in the relevant studies, was purchased from the National Centre for Cell Sciences (NCCS, Pune, India). These cell lines were maintained in Dulbecco's Modified Eagle's Medium (DMEM) (Invitrogen, USA), supplemented with 10% fetal bovine serum (Gibco BRL, Gaithersburg, MD), L-glutamine, and antibiotics (penicillin, 100 U/ml and streptomycin, 50μg/ml). Cells were cultured at 37°C in 95% air and 5% CO_2 humidified incubators. Cells were typically grown to 60-70% of confluency, washed in phosphate-buffered saline (PBS) and placed into serum-free medium (DMEM containing 0.1% bovine serum albumin) overnight prior to treatments [14, 15]. Sodium arsenite and arsenite tagged IONPs were dissolved with glass-distilled water to desired concentrations and passed through 0.45 μm Millipore filters (Millipore India Pvt. Ltd., Bangalore, India) to remove particulate matter and freshly prepared for each experiment.

2.8. Assessment of cell morphology

Cells (3×10^4/well), grown in 6-well plates in DMEM supplemented with 10% FBS for 24 h, were treated with $NaAsO_2$, IONPs and MCNPs in presence of magnetic field. Morphological changes were observed with an inverted microscope (OLYMPUS IX 70, Olympus Optical Co. Ltd., Sibuya-ku, Tokyo, Japan) and images were acquired.

2.9. Cell viability assay

Cell viability assay was performed using MTT dye. Briefly, $1x10^5$ cells were seeded per well in 100 ml of medium in 96-well microtiter plates (Nunc, Roskilde, Denmark). Cells grown for 24 h were exposed to $NaAsO_2$, IONPs and MCNPs in presence of external magnetic field. After 24 h of incubation, the medium was aspirated; MTT solution (1.2 mg/ml) added to each well and incubated for 4 h at 37°C. For solubilization of the formazan crystals formed, DMSO (100 µl) was added to each well and optical density was measured at wavelength 595 nm (EMax Precision Micro Plate Reader, Molecular Devices, USA). The absorbance correlates linearly to the number of living cells in culture. The percent cell survival was calculated as: Survival = (HepG2 test/HepG2 control) x 100%. Dose-response bar diagrams were drawn, and IC_{50} value, the concentration that inhibits 50% of the growth of cells, was calculated.

2.10. DAPI staining assay for the detection of nuclear damage

For detection of nuclear damage or chromatin condensation by 4'-6-diamidino-2-phenylindole (DAPI) staining, cells were either untreated or treated with $NaAsO_2$, IONPs and MCNPs in presence of magnetic field for 24 h. Cells were grown on coverslips in 6 cm petridishes till confluency. Coverslips were then withdrawn, washed with 0.1 M PBS and cells fixed in methanol for 10 min at room temperature. Cells were then stained with DAPI

(Sigma-Aldrich, USA) (10 µg/ml in PBS) for 20 min, washed twice with PBS and the coverslips mounted on a glass slide. Nuclear morphology was then observed by fluorescence microscope (OLYMPUS IX 70, Olympus Optical Co. Ltd., Sibuya-ku, Tokyo, Japan) and images were then acquired with excitation and emission wavelengths of 488 and 550 nm respectively. Apoptotic nuclei can be identified by the condensed chromatin or fragmented morphology of nuclear bodies.

2.11. Quantification of apoptosis using Annexin-V

Apoptosis was assayed by using an Annexin-V FITC apoptosis detection kit (Calbiochem, CA, USA). Briefly, cells were treated with or without $NaAsO_2$, IONPs and MCNPs, then washed and stained with PI and Annexin-V-FITC in accordance with the manufacturer's instructions. The percentages of live, apoptotic and necrotic cells were determined by flow cytometric method (LSR Fortessa^{TM} ,Beckton Dickinson, San Jose, CA, USA). Data from 10^6 cells were analyzed for each sample.

2.12. Cell cycle assay

For cell cycle assay, HepG2 cells were seeded at a density of 1 x 10^6 and exposed to $NaAsO_2$, IONPs and MCNPs in presence of magnetic field for 24 h. Following incubation, cells were collected and fixed in 70% ethanol for 24 h at 4°C. The cells were centrifuged (1,500g); cell pellet was resuspended in PBS (400 µl), RNaseA (10 mg/ml, 50 µl) and PI (2 mg/ml, 10 µl). The mixture was incubated in the dark at 37°C for 30 min and was then acquired and analysed by flow cytometry.

2.13. ROS detection assay

ROS were detected using the cell-permeable fluorescentprobe 2'-7'-dichlorofluorescein-diacetate (H_2DCFDA) (Sigma-Aldrich, USA), a non-fluorescent compound, which is

converted into highly fluorescent dichlorofluorescein (DCF) by cellular peroxides. Briefly, HepG2 cells were exposed to various agents for the indicated times and then loaded with H_2DCFDA (20 μM). Following incubation at 37°C for 30 min, cells were washed with PBS and fluorescence monitored in flow cytometric method at excitation wavelength of 488 nm and emission wavelength of 530 nm.

2.14. Mitochondrial membrane potential (MMP / $\Delta\Psi m$) measurement assay

Cells were treated with drugs for 24 h and MMP was measured with the voltage-sensitive lipophilic cationic fluorescent probe JC-1 (5,5',6,6'-tetrachloro-1,1',3,3'-tetraethylbenzimidazolcarbocyanine iodide). JC-1 monomers fluorescence red in stable mitochondria and upon exclusion combines to form green fluorescent dimers. Briefly, cells were collected; washed with cold PBS, incubated with JC-1 (5μg/ml) for 15min and analyzed by flow cytometric method.

2.15. Confocal microscopy

The effect of $NaAsO_2$, IONPs and MCNPs in presence of magnetic field nuclear translocation of p53 was measured by immunocytochemical analysis. HepG2 cells cultured on chambered plastic slides were fixed with ethanol for 30 min at 4°C and the detergent was extracted with 3% Triton X-100 for 10 min at room temperature. After washing with PBS and blocking with 3% bovine serum albumin (BSA) for 30 min, samples were incubated overnight with a primary antibody at 4°C. Excess primary antibody was removed by washing with PBS and samples were incubated with FITC-conjugated secondary antibody for 2 h at room temperature. After washing with PBS, slides were mounted using DAPI to visualize the nuclei. Specimens were covered with cover slips and evaluated under an Andor spinning Disc laser scanning confocal microscope.

3. Results and discussion

3.1 Synthesis and purification of arsenite tagged magnetic core-shell nanoparticles

For the formation of our MCNPs, we chose magnetic iron oxide nanoparticles (Fe_3O_4) as our core, as these iron oxide nanoparticles (IONPs) due to their significantly higher magnetic susceptibility, can afford magnetic properties at much lower concentrations. As such, we first synthesized these IONPs by co-precipitation method of a mixture of Fe^{2+} and Fe^{3+} in the presence of the nitrogen atmosphere citrate as a stabilizer, using a modified version of a previously reported method [16]. These IONPs were then coated with a thin layer of arsenite by injecting sodium arsenite solution into a sealed conical flux containing IONP solution at 72°C temperature under nitrogen atmosphere. The resulting solution was then stirred for two hours keeping the above temperature, which resulted in the formation of water-soluble MCNPs.

3.2. Characterization of IONPs and MCNPs

A detailed characterization of the IONPs and Fe_3O_4@As (MCNP) were then performed. First, dynamic light scattering (DLS) analysis revealed that the average diameter of IONP was 42 nm, which increased to 61 nm for the MCNPs (Fig. S1). Atomic force microscopy (AFM) analysis showed that the overall diameter increased from 40±1.0 nm to 58±1.0 nm for the IONPs and MCNPs respectively (Fig. 2). AFM analysis showed to some extent lower diameter value with respect to DLS analysis, since DLS measurement provides hydrated size of the nanoparticles. The arsenite layer onto the IONP core can clearly be seen in the three different modes of AFM images (Fig. 2).

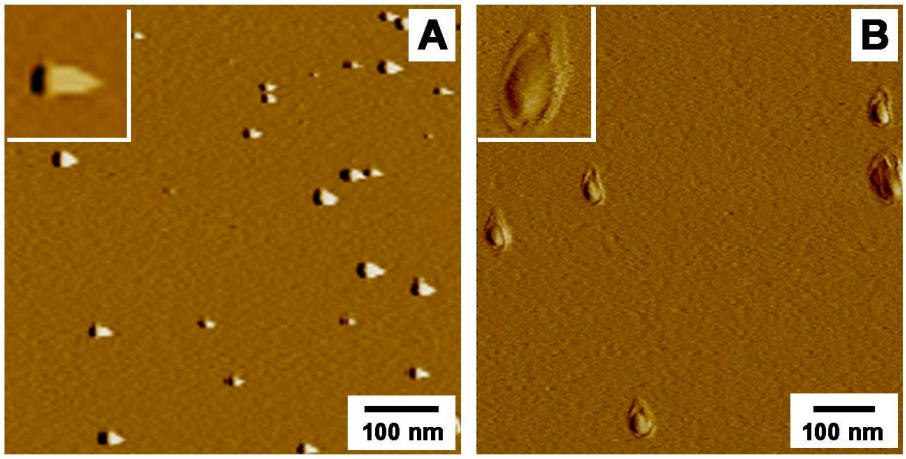

Fig. 2 AFM images of IONPs and MCNPs. The image A and B represent the amplitude flattened images for IONPs and MCNPs, respectively. The image B shows the formation of distinct layer of arsenite in MCNP. The inset represents magnified version of a single IONP or MCNP.

FTIR spectra (Fig. S2) of MNPs exhibit strong bands in the low frequency region (1000-400 cm^{-1}) due to the iron oxide skeleton. In other regions, the spectra of iron oxide have weak bands. The band at 582 cm-1 is assigned to the stretching mode of Fe-O and 427 cm^{-1} for lattice mode of FeO_6 indicating the formation of magnetite Fe_3O_4 [17]. The absorption bands at 1403 and 1617 cm^{-1} normally comes from carbon dioxide which generally nanomaterials absorbed from the environment due to their mesophorous structure. The arsenite shell formation onto the IONP core was again confirmed from FTIR analysis of IONPs and MCNPs respectively. In normal condition IONPs are surrounded by water molecules and/or closely spaced hydroxyl groups, which was characterized by the appearance of broad peak at 3379 cm^{-1} in the FTIR spectrum. In contrary, the FTIR spectrum of MCNPs did not show any intense peak at the wavelength of 3300 cm^{-1}. This difference is attributed to the deposition of arsenite onto the surface of magnetic core (Fe_3O_4). Here the core-shell formation was facilitated owing to the strong hydrogen bonding and ionic interaction of the hydroxyl groups, present at the surface of MNPs, with arsenite which results the

disappearance of 3379 cm^{-1} peak in the FTIR spectrum of MCNPs. Moreover, AFM images of IONPs showed some agglomerating nature, which is due to the strong internal hydrogen bonding of closely spaced hydroxyl groups on to the surface of IONPs. On the other hand, lack of this strong internal hydrogen bonding due to the formation of arsenite shell, MCNPs showed monomeric structures in their AFM images.

X-Ray diffraction patterns of both IONPs and MCNPs were shown in (Fig. S3). The appearance of sample diffraction peaks at 2θ = 30.17°, 35.71°, 43.32°, 53.59°, 57.11°, and 62.9° corresponded to the (220), (311), (400), (422), (511) and (440) crystal planes of IONP respectively, indicating that the resulting particles were Fe_3O_4 and magnetite in nature, with structures of cubic crystal having lattice parameter a_0 = 8.3952 Å. The shifting of the peaks in the XRD pattern of MCNPs indicates the coating of arsenite onto the IONPs.

3.3. MCNPs treatment under magnetic field sensitizes malignant HepG2 cells in vitro

The biological activity of $NaAsO_2$, IONPs and MCNPs was evaluated using human hepatocellular liver carcinoma cell line HepG2 in presence and absence of the external magnetic field. HepG2 cells treated only with $NaAsO_2$ in presence and absence of magnetic field, at clinically obtainable concentration (2 μM), showed cell growth inhibition of 2% at 24 h (Fig. S4). This dose of $NaAsO_2$ is supposed to minimize toxicities seen with higher doses of arsenic

In absence of magnetic field, IONPs alone had very little effect on viability of HepG2 cells irrespective of the dose, whereas in presence of magnetic field, slight decrease (2-5%) in viability was observed at 2 μM and a decrease up to 9 % was observed at 10 μM (Fig. S4). This could be due to the penetration of higher number IONPs at higher concentration.

However, treatment of MCNPs containing 2 μM $NaAsO_2$ clearly facilitated MCNPs induced cytotoxicity in a dose-dependent manner in HepG2 cells (Fig. S4). Of interest,

$NaAsO_2$ at 2 μM shows no appreciable change in cell cytotoxicity, but when administered through MCNPs under magnetic field, results in remarkably increased cytotoxicity (Fig. S4)

Thus cell viability assay demonstrated that $NaAsO_2$ at 2 μM shows no appreciable change in cell cytotoxicity in presence or absence of magnetic field, but when administered through MCNPs under magnetic field, results in remarkably increase in cytotoxicity which is due to the ability of external magnetic field to target and localize the MCNPs more efficiently by means of magnetic field indused penetration of cell membrane.

3.4. Assessment of cell morphology and DNA damage

In presence of the external magnetic field HepG2 cells were treated with $NaAsO_2$, IONPs and MCNPs in different concentrations and observed under confocal microscope. Under the magnetic field, the characteristic apoptotic changes like cell rounding and cell shrinkage was found with the concentration of 2 and 5 μM $NaAsO_2$ containing MCNPs for 24 h, whereas $NaAsO_2$ alone did not show any morphological changes even at 5 μM (Fig. 3A-F). This is due to the magnetic field indused penetration of cell membrane. The decrease in cell proliferation could be due to the induction of apoptosis. To investigate whether MNCP-induced growth inhibition under external magnetic field was due to induction of apoptosis, HepG2 cells were incubated alone or treated with 5μM $NaAsO_2$ and 2 and 5 μM $NaAsO_2$ containing MCNP under external magnetic field and stained with DAPI. The majority of MCNPs treated cells displayed apoptotic features; including condensed nuclei and nuclear fragmentation in contrast to $NaAsO_2$, IONPs treated and untreated control cells (Fig. 3F-J). This result is in good agreement with the above cell viability assessment by MTT.

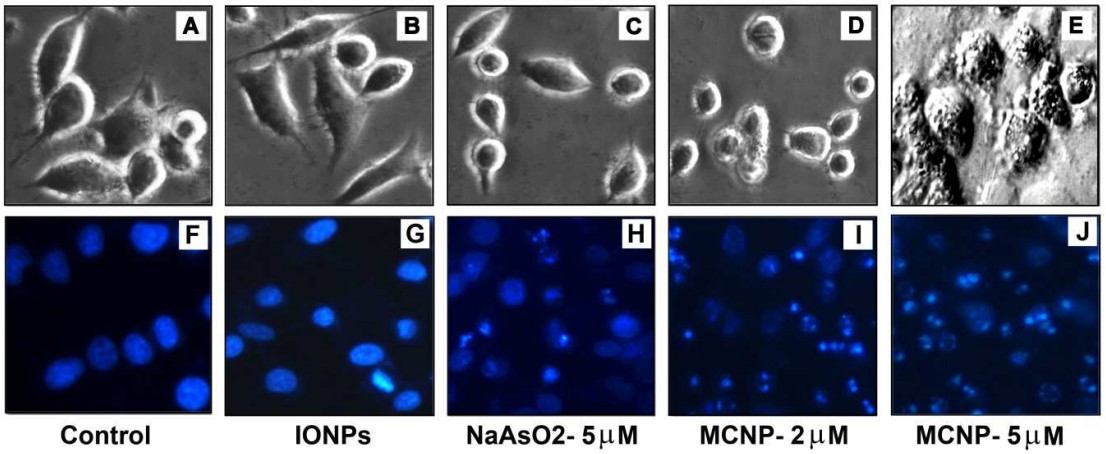

Fig. 3 Cellular morphology of HepG2 cells alone (A) and treated for 24 h with IONPs (B), 5μM $NaAsO_2$ (C), 2 and 5μM $NaAsO_2$ containing MCNPs (D, E). The lower panel shows nuclear morphology by DAPI staining of control HepG2 cells (F) and following IONPs (G), 5μM $NaAsO_2$ (H), 2 and 5μM $NaAsO_2$ containing MCNPs (I,J) treatment for 24 h as observed under fluorescence microscope.

3.5. Levels of apoptosis determined by annexinV/PI staining and FACS analysis

To confirm the apoptosis-inducing effect of MCNPs under magnetic field on HepG2 cells, we further stained the treated cells with Annexin-V-FITC / PI and analysed by flow cytometry (Fig. S5). The percentage of apoptotic cells were negligible in untreated control and in cells treated with IONP alone. When treated with 5μM $NaAsO_2$, the percentage of apoptotic cells increased to 20.4% which, however, resulted in an increase of 42.3% and 62.3% respectively upon treatment with 2 and 5μM $NaAsO_2$ containing MCNPs suggesting that MCNPs under magnetic field can induce apoptosis in HepG2 cells with higher rate and efficiency in comparison to pure $NaAsO_2$.

3.6. MCNP induced cell cycle arrest in HepG2 cells

Since arsenic-induced apoptosis is associated with cell cycle alterations [18], the cell cycle profile was further analyzed by measuring DNA content using PI staining. As shown in

(Fig.4), cells treated with the 2 and 5 μM $NaAsO_2$ containing MCNPs, have a significantly high percentage (80 &71%) of cells in the G0-G1 phase of the cell cycle, indicative of apoptotic cells, when compared to percentage of cells treated with only $NaAsO_2$ (62%).

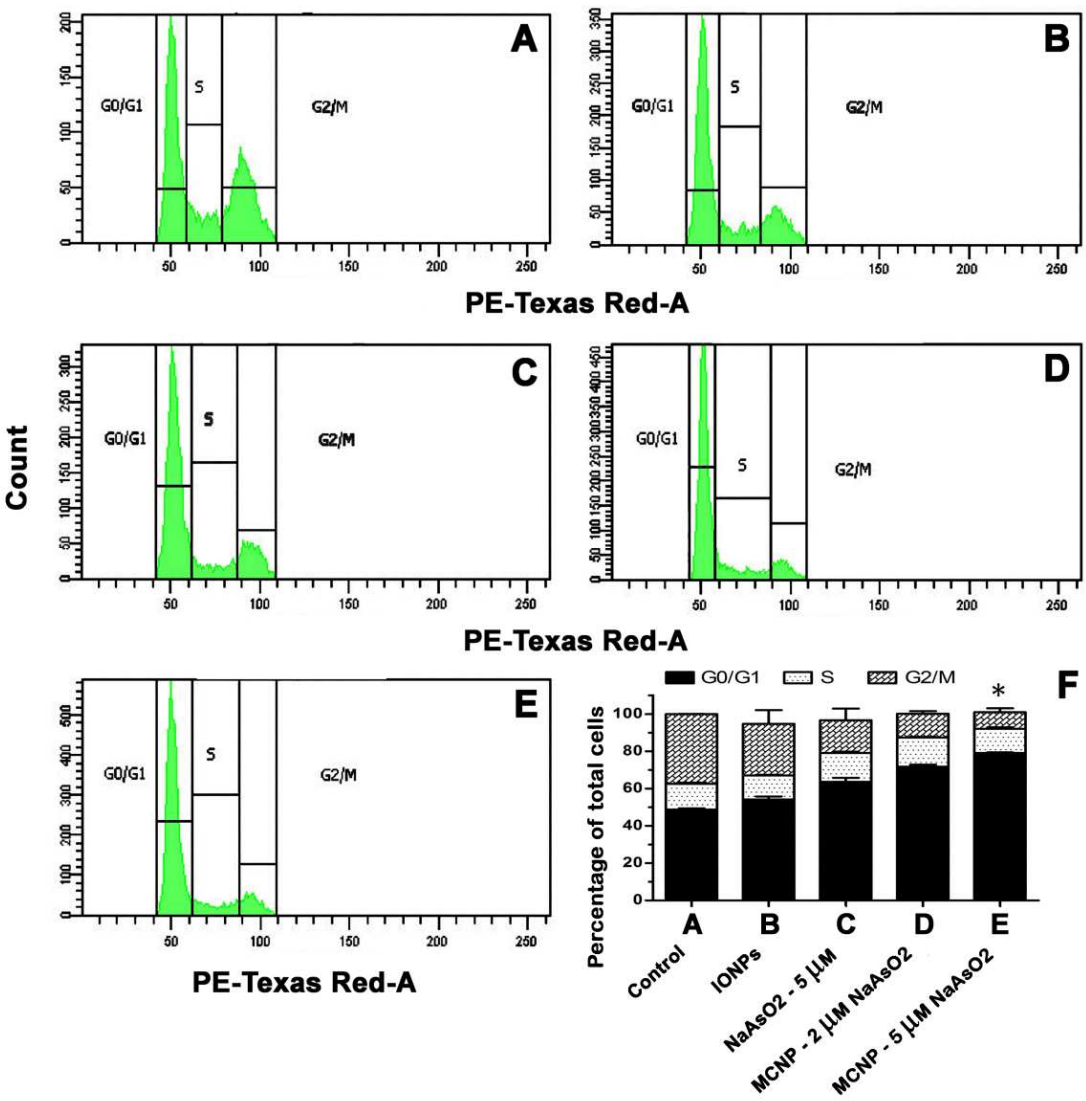

Fig. 4 Cell cycle histograms of the DNA content of HepG2 cells untreated or treated with IONPs, 5μM $NaAsO_2$, 2 and 5μM $NaAsO_2$ containing MCNPs for 24 h. The DNA content was determined by flow cytometry after staining with PI. The percentage of cells, found in G0/G1 region, represents the proportion of apoptotic cells. All results represent the mean of three independent experiments and the bar diagram corresponds to the mean ± SD of apoptotic cells obtained from those three experiments. The symbol * denote statistical significance ($P < 0.05$).

3.7. MCNPs under magnetic field elevates ROS production in HepG2 cells

Apoptosis is an important path ways to destroy the cancer cells. Excessive ROS generation is one of the potent causes to induce apoptosis leading to the cell death through the damage of cellular proteins, lipids and DNA [19, 20]. To explore the molecular mechanism for the effect of MCNPs, we investigated whether these drugs induce the generation of reactive oxygen species (ROS). The ROS generation was measured by flow cytometry using the fluorescent indicator H2DCFDA. In contrast to control, 5 µM $NaAsO_2$ containing MCNPs treatment in HepG2 cells induced about 2-fold increase in mean fluorescence, which is higher compared to treatment with 5 µM $NaAsO_2$ alone, indicating higher ROS generation ability of MCNPs under magnetic field directed targeting (Fig. 5).

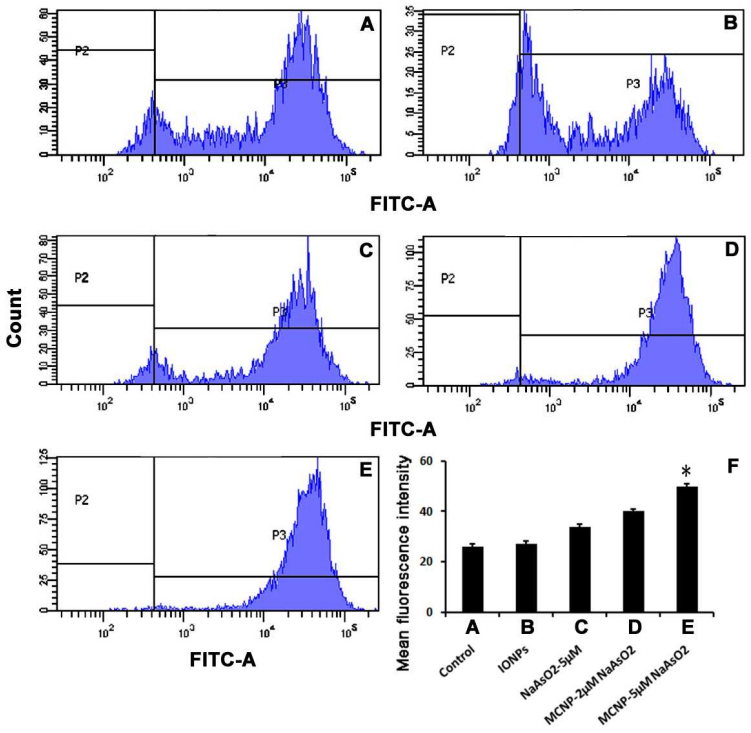

Fig. 5 Flow cytometric determination of DCF fluorescence as a measure of intracellular ROS in HepG2 cells untreated or treated with IONPs, 5µM $NaAsO_2$, 2 and 5µM $NaAsO_2$ containing MCNPs for 24 h. The change in mean fluorescence intensity (MFI) ± standard deviation from three independent experiments is represented as bar diagram.

3.8. MCNPs induced mitochondrial transmembrane potential collapse

Collapse of mitochondrial membrane potential (MMP) before cell killing, is a hallmark for apoptosis. HepG2 cells, treated with the 2 and 5 μM $NaAsO_2$ containing MCNPs under magnetic field, were found to undergo a more dramatic MMP depolarization (a drastic decrease in JC-1 monomer red fluorescing cell population) when compared to arsenic and IONPs alone, as detected by flow cytometry with JC-1 staining, indicating higher degree of MMP disruption ability of MCNP (Fig. 6).

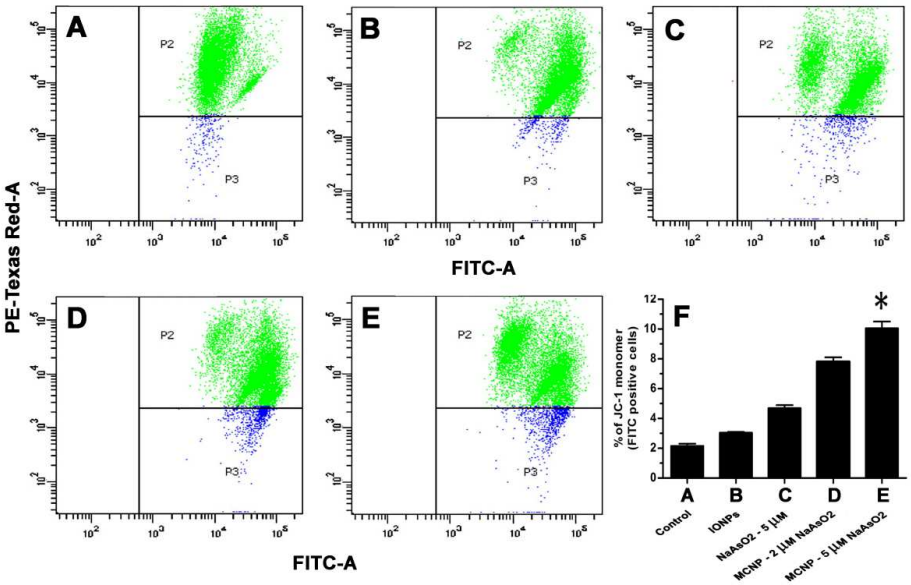

Fig. 6 Assessment of mitochondrial membrane potential using JC-1 dye in untreated HepG2 cells or cells treated with IONPs, 5μM $NaAsO_2$, 2 and 5μM $NaAsO_2$ containing MCNPs for 24 h. The change in fluorescence intensity ± standard deviation from three independent experiments is represented as bar diagram.

3.9. MCNPs induced nuclear localization of p53 indicating apoptosis

The p53 tumour suppressor protein is well known to respond to DNA damage by inducing either G1 arrest or apoptosis. Under normal conditions of cell growth, the p53 protein exists

in cytoplasm and is inactive for many functions, including the transactivation of specific target genes.

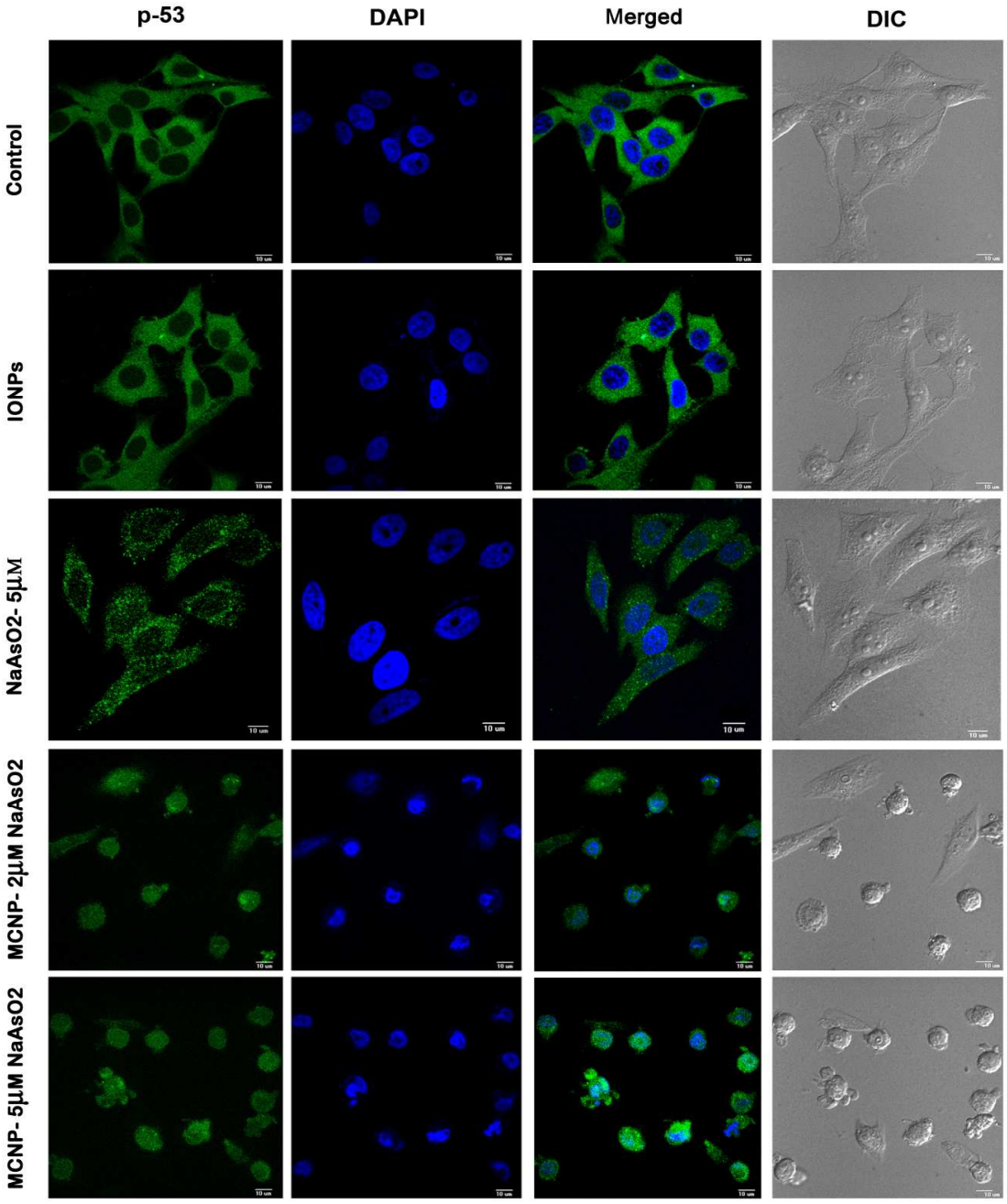

Fig. 7 Localization of p53 in HepG2 cells during apoptosis. DAPI was used to stain the nuclei (blue) and localization of p53 (green) within HepG2 cells was examined by confocal microscopy before and after treatment with IONPs, 5µM NaAsO2, 2 and 5µM NaAsO2 containing MCNPs.

Since p53 helps to repair DNA damage, under apoptotic condition, p53 express largely and translocated in the nuclear part. The sensitivity of p53 as a DNA damage sensor is remarkable and it have shown that a single double strand break in DNA may be sufficient to trigger a p53 response [21]. Our results demonstrate that the untreated and only IONP treated HepG2 cells showed localization of p53 (developed with FITC-labeled secondary antibodies) in cytoplasm under magnetic field, indicating no apoptosis or DNA damage (Fig. 7). In contrast, 2 and 5 μM $NaAsO_2$ containing MCNPs treatment under magnetic field for 24 h showed clear nuclear localization of p53 as compared to the partial localization upon treatment with 5 μM $NaAsO_2$ alone. All the above observations support to consider arsenite containing MCNPs as a good anticancer agent under external magnetic field directed targeting and also helps to construct a putative pathway involved in MCNP induced apoptosis (Fig. 8).

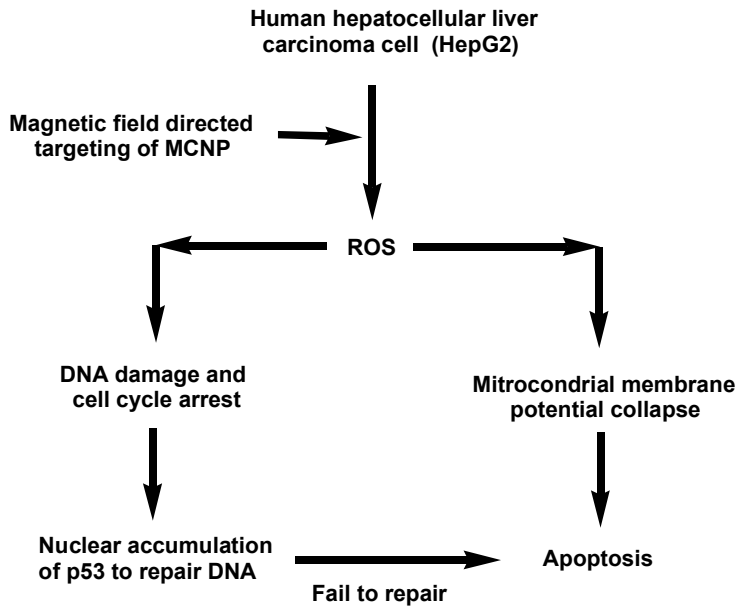

Fig. 8 Schematic representation of the probable pathway involved in $NaAsO_2$ containing MCNP-induced apoptosis in HepG2 cells.

4. Conclusions

In conclusion, we have synthesized a well-defined magnetic core-shell nanoparticles (MCNPs), composed of a highly magnetic core (Fe_3O_4) surrounded by a thin arsenite shell ($NaAsO_2$). These MCNPs could deliver sodium arsenite into human hepatocellular carcinoma (HepG2) cells in a highly efficient and external magnetically controlled manner. In particular, although MCNPs have been utilized for the efficient targeting of various drugs, this is the first demonstration of delivery of sodium arsenite to cancerous cells by utilization of magnetic property of MCNPs. Moreover, previous studies have shown that sensitization of various cancerous cells requires up to 10-fold higher dose of arsenic which is not clinically achievable without the risk of arsenic-mediated side effects or damage to normal cells as the maximum tolerance dose limit is ~ 2 μM. Here we have demonstrated that 2 μM arsenite containing MCNPs, under magnetically control targeting, was able to induce apoptosis in HepG2 cells as evidenced by DAPI staining, Annexin V-PI staining and Cell cycle analysis following intrinsic apoptotic pathway. This apoptosis was mediated through ROS generation as evident by ROS generation assay, mitochondrial membrane potential disruption, DNA damage and nuclear localization of p53. To our knowledge, this is the first report to indicate the association of p53 with arsenic containing MCNP-induced hepatocellular apoptosis. Besides, being magnetic in nature, MCNP may allow for use as an MRI contrast agent in the future to track MCNP targeted cells in vivo. Thus, the MCNP-based drug targeting method can potentially be a powerful tool for the treatment of various cancers.

Acknowledgments

This study is supported by the Council of Scientific and Industrial Research (CSIR, Govt of India). S.M is the recipient of UGC-NET fellowship and S.D, N.C is the recipient of CSIR-SRF. Authors express sincere thanks to Dr. Suvendra Nath Bhattacharyya and Mr. Diptodeep

Sarkar for his assistance during Confocal Microscopic analysis. Authors also would like to thank Ms. Anusila Ganguly, Mr. Muruganandan and Mr. Satyabrata Samadder of IICB for their assistance during the Flow Cytometric study, AFM and FTIR experiments respectively. We thank the anonymous reviewers for their critical comments that enabled us to improve the manuscript.

Supplementary data

Size distribution curve of IONPs and MCNPs by dynamic light scattering, FTIR spectra of IONPs and MCNPs, XRD spectra of IONPs and MCNPs, Cytotoxic effect of IONPs, NaAsO2, and MCNPs on HepG2 cell at different concentration and in absence and presence of magnetic field, apoptosis determination by annexinV/PI staining.

References

1. X. M. Hu, T. Hirano and K. Oka, *Cancer Chemother Pharmacol*, 2003, **51**, 119-126.

2. J. Y. Jiang, A. L. Li, G. M. Wang, J. B. Ma, J. Hao, Z. Q. Guan and S. S. Xie, *Zhongguo Shi Yan Xue Ye Xue Za Zhi*, 2003, **11**, 633-638.

3. N. Larochette, D. Decaudin, E. Jacotot, C. Brenner, I. Marzo, S. A. Susin, N. Zamzami, Z. Xie, J. Reed and G. Kroemer, *Experimental Cell Research*, 1999, **249**, 413-421.

4. I. Ora, L. Bondesson, C. JÃ¶nsson, J. Ljungberg, I. PÃ¶rn-Ares, S. Garwicz and S. PÃ¥hlman, *Biochemical and Biophysical Research Communications*, 2000, **277**, 179-185.

5. W. H. Park, J. G. Seol, E. S. Kim, J. M. Hyun, C. W. Jung, C. C. Lee, B. K. Kim and Y. Y. Lee, 2000, vol. 60, pp. 3065-3071.

6. C. Perkins, C. N. Kim, G. Fang and K. N. Bhalla, 2000, vol. 95, pp. 1014-1022.

7. Z. Y. Shen, J. Shen, W. J. Cai, C. Hong and M. H. Zheng, 2000, **5** 155-163.

8. J. J. Li, Q. Tang, Y. Li, B. R. Hu, Z. Y. Ming, Q. Fu, J. Q. Qian and J. Z. Xiang, *Acta Pharmacol Sin*, 2006, **27**, 1078-1084.

9. R. Chowdhury, S. Chowdhury, P. Roychoudhury, C. Mandal and K. Chaudhuri, *Apoptosis*, 2009, **14**, 108-123.

10. R. Q. Huang, S. F. Gao, W. L. Wang, S. Staunton and G. Wang, *Sci Total Environ*, 2006, **368**, 531-541.

11. A. M. Bode and Z. Dong, *Crit Rev Oncol Hematol*, 2002, **42**, 5-24.

12. S. Mandal, M. Hossain, T. Muruganandan, G. S. Kumar and K. Chaudhuri, *RSC Advances*, **3**, 20793-20799.

13. S. Mandal, M. Hossain, P. S. Devi, G. S. Kumar and K. Chaudhuri, *J Hazard Mater*, **248-249**, 238-245.

14. N. Chatterjee, S. Das, D. Bose, S. Banerjee, S. Das, D. Chattopadhyay and K. D. Saha, *Toxicol Appl Pharmacol*, **264**, 182-191.

15. S. Das, N. Chatterjee, D. Bose, S. K. Dey, R. N. Munda, A. Nandy, S. Bera, S. K. Biswas and K. Das Saha, *Cell Physiol Biochem*, **29**, 251-260.

16. S. Kayal and R. V. Ramanujan, *Materials Science and Engineering: C*, **30**, 484-490.

17. A. S. Al-Kady, M. Gaber, M. M. Hussein and e.-Z. M. Ebeid, *Spectrochimica acta. Part A, Molecular and biomolecular spectroscopy*, **83**, 398-405.

18. S. C. McNeely, B. F. Taylor and J. C. States, *Toxicol Appl Pharmacol*, 2008, **231**, 61-67.

19. I. G. Kirkinezos and C. T. Moraes, *Seminars in Cell & Developmental Biology*, 2001, **12**, 449-457.

20. T. Ozben, *Journal of Pharmaceutical Sciences*, 2007, **96**, 2181-2196.

21. L. C. Huang, K. C. Clarkin and G. M. Wahl, *Proc Natl Acad Sci U S A*, 1996, **93**, 4827-4832.